# Model-Dependent Prosthesis Control with Real-Time Force Sensing

Rachel Gehlhar, Je-han Yang, and Aaron D. Ames

Abstract—Lower-limb prosthesis wearers are more prone to fall than non-amputees. Powered prostheses can reduce this instability of passive prostheses. While shown to be more stable in practice, powered prostheses generally use modelindependent control methods that lack formal guarantees of stability and rely on heuristic tuning. Recent work overcame one of the limitations of model-based prosthesis control by developing a class of stable prosthesis subsystem controllers independent of the human model, except for its interaction forces with the prosthesis. Our work realizes the first modeldependent prosthesis controller that uses in-the-loop on-board real-time force sensing at the interface between the human and prosthesis and at the ground, resulting in stable humanprosthesis walking and increasing the validity of our formal guarantees of stability. Experimental results demonstrate this controller using force sensors outperforms the controller when not using force sensors with better tracking performance and more consistent tracking performance across 4 types of terrain.

### I. Introduction

Lower-limb prosthesis users fall more frequently than non-amputees [1]. A survey in [2] found 45% of polled amputees had fallen in the past year while wearing their prosthesis. This instability could be due to their passive prostheses, which can be less stable than powered prostheses [3]. Current powered prosthesis control methods tend to be model-independent [4], [5], requiring heuristic tuning, lacking formal guarantees of stability, and not utilizing the system's natural dynamics. Current state of the art controllers tune impedance parameters for multiple discrete phases of a gait cycle for different subjects and behaviors [6]-[8] Modelbased control methods hold potential to yield a more transferable method between devices, users, and behaviors since they rely on measurable model parameters and inputs instead of a large set of heuristic tuning parameters. Additionally, modelbased methods can be designed to yield formal guarantees of stability since they are based on the actual system dynamics. This motivates developing model-based prosthesis control methods that lend a more transferable method between applications and guarantee stability for the user.

A challenge arises in developing model-dependent prosthesis controllers: the human dynamics are unknown. The work of [9] addressed this limitation by developing rapidly

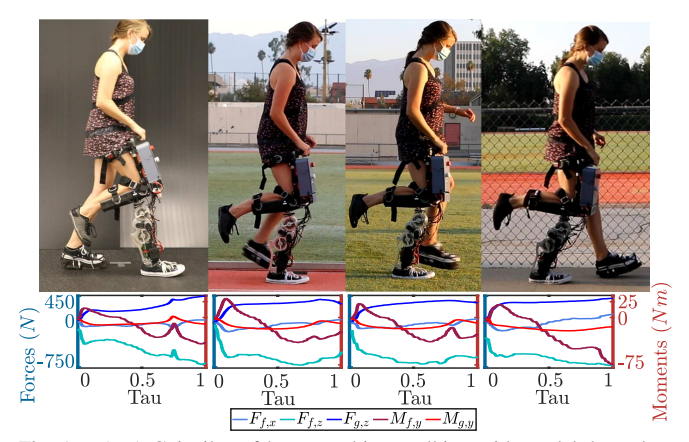


Fig. 1. (top) Gait tiles of human subject walking with model-dependent prosthesis controller using real-time force measurements on four terrains: rubber floor, outdoor track, grass, and sidewalk. (bottom) Measured socket and ground force profiles during stance for respective terrain.

exponentially stabilizing control Lyapunov functions (RES-CLFs), which were shown to stabilize bipedal robotic walking [10], in the context of separable systems [11], [12]. This resulted in a class of stabilizing prosthesis controllers relying only on local prosthesis information. Previously, RES-CLFs were difficult to realize on hardware due to the typical required inversion of the inertia matrix which is computationally expensive and susceptible to error. The work of [13] developed and demonstrated a RES-CLF controller on a bipedal robot without inverting the inertia matrix by constructing the RES-CLF in an inverse dynamics framework in a quadratic program (QP) [14]. The work of [13] brings the class of controllers developed in [9] closer to being implementable.

Realizing RES-CLF controllers on prostheses meets an additional challenge: they require knowledge of both the ground reaction forces and moment and socket interaction forces and moment. (For simplicity we refer to these as "GRFs" and "socket forces".) The work of [15] realized the first model-dependent prosthesis controller in stance with consideration for the forces, using holonomic constraints for the GRFs and force estimation for the socket forces. However using holonomic constraints to determine GRFs assumes a rigid contact with the ground, inaccurately representing many real-life scenarios where the terrain deforms under a load, like granular media [16]. Developing control methods accounting for non-rigid terrain is especially important for prostheses to enable amputees to walk stably on a variety of surfaces present in daily life. Additionally, this method only estimated the socket forces which may not accurately capture the varying load a user applies during stance. To more accurately account for the prosthesis system dynamics in model-dependent control, force sensors are needed.

<sup>\*</sup>This material is based upon work supported by the National Science Foundation Graduate Research Fellowship under Grant No. DGE-1745301. This research was approved by California Institute of Technology Institutional Review Board with protocol no. 16-0693 for human subject testing.

R. Gehlhar and A. Ames are with the Department of Mechanical and Civil Engineering, J. Yang is with the Department of Electrical Engineering, California Institute of Technology, Pasadena, CA 91125 USA. Emails: {rgehlhar, ames, jyang5}@caltech.edu

Load cells have been incorporated into powered prosthesis platforms to detect ground contact, GRFs, and center of pressure (CoP) [5], [17], [18]. The work of [17], used GRF sensing capability to determine motion intent to trigger transitions between gait phases of finite-state based impedance control. The work of [5] used the CoP to encode and modulate virtual constraints for prosthesis control. However, to date, GRF and socket force measurements have not been included in the modeled dynamics to achieve modeldependent prosthesis control. Additionally, to the best of the authors' knowledge, GRFs and CoP measurements from an insole plantar pressure sensor have not been utilized as real-time feedback in prosthesis control [19]. This work integrates a load cell, insole pressure sensor, and an IMU on a transfemoral powered prosthesis platform, Fig. 1, to realize the first model-dependent prosthesis controller that uses realtime force sensing to complete the dynamics, resulting in stable human-prosthesis walking.

In this paper, Section II overviews separable system control methods and RES-CLFs. Section III constructs the controller of focus in this work that utilizes real-time force and inertial measurement unit (IMU) measurements. Following, Section IV defines the amputee-prosthesis model and describes the gait generation method. Section V presents the selection criteria, hardware specifications, and software implementation details of the pressure sensor used in this study. This pressure sensor is integrated into the powered transfemoral prosthesis platform, AMPRO3, which is described in Section VI, followed by the experimental set-up. Finally, the experimental results show the improved tracking performance with this real-time force feedback for 4 types of terrain. The main contributions of this paper are

- integrating an insole pressure sensor into a powered prosthesis platform for real-time GRF sensing and to enable future gait analysis and CoP control methods
- realizing the first model-dependent prosthesis controller in stance and non-stance phases with in-the-loop onboard real-time force sensing at the ground and socket
- achieving improved tracking performance consistent across 4 terrains.

## II. BACKGROUND ON SEPARABLE SUBSYSTEMS

To construct the controller used as the focus of this work and justify our claim of formal guarantees of stability for the whole human-prosthesis system, we will provide a brief overview of the separable subsystem framework along with RES-CLFs starting in the context of robotic control systems.

**Robotic Control System.** Consider a robotic control system in 2D space with  $\eta$  DOFs and configuration coordinates  $q=(q_l^T,q_f^T,q_s^T)^T\in\mathbb{R}^\eta$  defining the configuration space  $\mathcal{Q}$ . We will focus on a subsystem of the robot defined by coordinates  $q_s\in\mathbb{R}^{\eta_s}$  with  $m_s$  actuators. The remaining system is defined by  $q_l\in\mathbb{R}^{\eta_l}$  with  $m_r$  actuators. The attachment point between these systems is modeled as a 3-DOF rigid joint (x,z) Cartesian position, and pitch) and defined with coordinates  $q_f$ . Here  $\eta_l+\eta_s+3=\eta$  and  $m_s+m_r=m$ , the total number of actuators. The coordinates

 $q_l$  include the floating base coordinates  $q_B \in \mathbb{R}^3$ . The constrained dynamics of the full system are given by the following Euler-Lagrange equation [20]:

$$D(q)\ddot{q} + H(q,\dot{q}) = Bu + J_h^T(q)\lambda_h \tag{1}$$

$$J_h(q)\ddot{q} + \dot{J}_h(q,\dot{q})\dot{q} = 0, \tag{2}$$

where D(q) is the inertia matrix,  $H(q,\dot{q})$  is a vector containing Coriolis, centrifugal, and gravity forces, B is the actuation matrix for  $u \in \mathbb{R}^m$  control inputs, and  $J_h(q)$  is the Jacobian of the holonomic constraints h(q) and projects the constraint wrenches  $\lambda_h$ .

**Robotic Subsystem.** To develop model-based prosthesis subsystem controllers, we model the robotic *subsystem* separately with floating base coordinates  $\bar{q}_B \in \mathbb{R}^3$  where it attaches to the remaining system. With subsystem configuration coordinates  $\bar{q} = (\bar{q}_B^T, q_s^T)^T \in \mathbb{R}^{\bar{\eta}}$ , where  $\bar{\eta} = \eta_s + 3$ , the constrained robotic subsystem dynamics are:

$$\bar{D}(\bar{q})\ddot{\bar{q}} + \bar{H}(\bar{q},\dot{\bar{q}}) = \bar{B}u_s + \bar{J}_h^T(\bar{q})\bar{\lambda}_h + \bar{J}_f^T(\bar{q})F_f \quad (3)$$

$$\bar{J}_h(\bar{q})\dot{\bar{q}} + \dot{\bar{J}}_h(\bar{q},\dot{\bar{q}})\dot{\bar{q}} = 0. \tag{4}$$

Here  $F_f$  are the fixed joint interaction forces inputted to this system and projected into the dynamics by  $\bar{J}_f(q)$ .  $\bar{J}_h(\bar{q})$  is the Jacobian of the  $\bar{\eta}_h$  subsystem holonomic constraints  $\bar{h}(\bar{q})$  with constraint wrench  $\bar{\lambda}_h$ . By solving for  $\bar{q}$  in the dynamics (3) and substituting this into the holonomic constraint equation (4), we solve for the constraint wrenches:

$$\bar{\lambda}_h = (\bar{J}_h \bar{D}^{-1} \bar{J}_h^T)^{-1} (\bar{J}_h \bar{D}^{-1} (\bar{H} - \bar{B}u_s - \bar{J}_f^T F_f) - \dot{\bar{J}}_h \dot{q}). \quad (5)$$

For the prosthesis, the work of [15] used (5) to calculate the GRFs modeled as holonomic constraints with the ground, estimated the fixed joint force  $F_f$ , and calculated  $\bar{q}_B$  and  $\dot{q}_B$  in stance based on inverse kinematics. For this paper we use the x-direction holonomic constraint to calculate the x-direction GRF but use a pressure sensor to measure the other GRFs: z-direction force and y-direction moment. A load cell measures the fixed joint socket forces  $F_f$  and an IMU to measures  $\bar{q}_B$  and  $\dot{q}_B$  in non-stance.

**Separable Subsystems.** With states  $x_q = (q^T, \dot{q}^T)^T$ , we write the full robotic system dynamics (1) as an ODE:

$$\dot{x}_{q} = \underbrace{\begin{bmatrix} \dot{q} \\ D^{-1}(q)(-H(q,\dot{q}) + J_{h}(q)^{T} \lambda_{h} \end{bmatrix}}_{f_{q}(x_{q})} + \underbrace{\begin{bmatrix} 0 \\ D^{-1}(q)(B) \end{bmatrix}}_{g_{q}(x_{q})} u.$$

To apply the *separable system* framework of [12], we rearrange the states and define  $x_r = (q_l^T, q_f^T, \dot{q}_l^T, \dot{q}_f^T)^T$  and  $x_s = (q_s^T, \dot{q}_s^T)^T$  which, due to the fixed joint as explained in [12], yields a system of the following form:

$$\begin{bmatrix} \dot{x}_r \\ \dot{x}_s \end{bmatrix} = \underbrace{\begin{bmatrix} f^r(x) \\ f^s(x) \end{bmatrix}}_{f(x)} + \underbrace{\begin{bmatrix} g^r_1(x) & g^r_2(x) \\ 0 & g^s(x) \end{bmatrix}}_{g(x)} \begin{bmatrix} u_r \\ u_s \end{bmatrix}, \tag{6}$$

$$x_r \in \mathbb{R}^{n_r}, \ x_s \in \mathbb{R}^{n_s}, \ u_r \in \mathbb{R}^{m_r}, \ u_s \in \mathbb{R}^{m_s}.$$

The remaining control input  $u_r$  does not affect the dynamics of  $x_s$ , allowing subsystem controller design with the  $x_s$ 

dynamics independent of the  $x_r$  dynamics. We define a *separable subsystem* and *remaining system* [9], [12], respectively,

$$\dot{x}_s = f^s(x) + g^s(x)u_s,\tag{7}$$

$$\dot{x}_r = f^r(x) + g_1^r(x)u_r + g_2^r(x)u_s. \tag{8}$$

**Equivalent Subsystem.** The subsystem dynamics still depend on the full system states so we alternatively express the dynamics of  $x_s$  as an ODE using (3) with a method similar to that used for the full-order dynamics:

$$\dot{\bar{x}}_s = \bar{f}^s(\mathcal{X}) + \bar{g}^s(\mathcal{X})u_s, 
\mathcal{X} = (\bar{x}_r^T, x_s^T, \zeta^T)^T \in \mathbb{R}^{\bar{n}}.$$
(9)

Here  $\bar{x}_s=x_s,\ \bar{x}_r=(\bar{q}_B^T,\bar{q}_B^T)^T\in\mathbb{R}^{\bar{n}_r}$  are measurable states, and  $\mathcal X$  is the vector of states  $\bar{x}=(\bar{x}_r^T,x_s^T)^T$  and measurable input  $\zeta=F_f\in\mathbb{R}^{n_f}$ . This system equates to (7) by a transformation  $T(x)=\mathcal X$ , where  $\bar{f}^s(\mathcal X)=f(x)$  and  $\bar{g}^s(\mathcal X)=g^s(x)$  for all x. For this robotic system form, this transformation exists and is given in [12]. An IMU and force sensor give  $\bar{x}_r$  and  $\zeta$  in practice.

**Separable Subsystem RES-CLF.** With the subsystem now defined in locally available coordinates  $\mathcal{X}$ , we define a class of stabilizing model-dependent subsystem controllers. Using the work of [9] we construct a RES-CLF  $\bar{V}^s_{\varepsilon}(x_s)$  for the equivalent subsystem,

$$\bar{c}_1^s \|x_s\|^2 \le \bar{V}_{\varepsilon}^s(x_s) \le \frac{\bar{c}_2^s}{\varepsilon^2} \|x_s\|^2$$

$$\inf_{u_s \in \mathbb{R}^{m_s}} [\dot{V}_{\varepsilon}^s(\mathcal{X}, u_s)] \le -\frac{\bar{c}_3^s}{\varepsilon} \bar{V}_{\varepsilon}^s(x_s),$$
(10)

for all  $0 < \varepsilon < 1$  and  $\mathcal{X} \in \mathbb{R}^{\bar{n}}$ , with constants  $\bar{c}_1^s, \bar{c}_2^s, \bar{c}_3^s > 0$ . All controllers that satisfy  $\dot{V}_{\varepsilon}^s(\mathcal{X}, u_s) \leq -\frac{\bar{c}_3^s}{\varepsilon} \bar{V}_{\varepsilon}^s(x_s)$  belong to the class  $\bar{K}_{\varepsilon}^s(\mathcal{X})$ :

$$\bar{K}_{\varepsilon}^{s}(\mathcal{X}) = \{ u_{s} \in \mathbb{R}^{m_{s}} : \dot{\bar{V}}_{\varepsilon}^{s}(\mathcal{X}, u_{s}) \leq -\frac{\bar{c}_{3}^{s}}{\varepsilon} \bar{V}_{\varepsilon}^{s}(x_{s}) \}. \quad (11)$$

The work of [10] developed RES-CLF controllers with  $\varepsilon$  to tune  $\varepsilon$  to yield fast enough convergence such that a hybrid system and its zero dynamics would not be destabilized by the impact dynamics of the hybrid system.

Main Theoretic Idea. By the work of [9], when a RES-CLF stabilizes the remaining system (8), any controller  $u_s \in \bar{K}^s_\varepsilon(\mathcal{X})$  stabilizes the full-order hybrid system with zero dynamics. Hence, separating a robotic system and constructing an equivalent subsystem provides a means to construct model-dependent subsystem controllers using solely local information guaranteeing full-order system stability while also utilizing the natural dynamics. In the case of a human-prosthesis system, we assume the human stabilizes itself based on research of central pattern generators which suggests biological walkers demonstrate stable rhythmic behavior [21], meaning they have limit cycles. All stabilizing controllers for these hybrid limit cycles belong to the class of RES-CLFs in [9] for the remaining system.

#### III. CONTROL METHODS

The ID-CLF-QP of [13] provides an implementable form of a RES-CLF. We outline this construction for an equivalent robotic subsystem (3) with the additional  $\bar{J}_f^T(\bar{q})F_f$  term in the dynamics. We explain how we measure this term, the GRFs, and the floating base coordinates for the prosthesis dynamics.

### A. Controller Formulation

To develop a Lyapunov function for the ID-CLF-QP of [13] we construct outputs to feedback linearize the system and dictate the motion of the robot.

**CLF Construction.** We define linearly independent subsystem positional outputs to enforce desired trajectories on the robotic subsystem,

$$y_s(x_s) = y_s^a(x_s) - y_s^d(\tau(x_s), \alpha),$$
 (12)

where  $y_s^a(x_s)$  are the actual joint outputs and  $y_s^d(\tau(x_s,\alpha))$  are the desired trajectories defined by parameters  $\alpha$  and modulated by  $\tau(x_s)$ , a state-based phase variable. Taking the derivatives along the equivalent subsystem dynamics (9), we relate the outputs to the control input  $u_s$ :

$$\ddot{y}_s = L_{\bar{f}^s}^2 y_s(\mathcal{X}) + L_{\bar{g}^s} L_{\bar{f}^s} y_s(\mathcal{X}) u_s.$$

Here  $L_{\bar{f}^s}^2 y_s(\mathcal{X})$  and  $L_{\bar{g}^s} L_{\bar{f}^s} y_s(\mathcal{X})$  denote the Lie derivatives [22]. Because the outputs are linearly independent,  $L_{\bar{g}^s} L_{\bar{f}^s} y_s(\mathcal{X})$  is invertible, making our system feedback linearizable [22] with feedback linearizing controller,

$$u_s(\mathcal{X}) = \left(L_{\bar{g}^s} L_{\bar{f}^s} y_s(\mathcal{X})\right)^{-1} \left(-L_{\bar{f}^s}^2 y_s(\mathcal{X}) + \nu\right), \quad (13)$$

with auxiliary control input  $\nu$ . This controller yields  $\ddot{y}_s = \nu$  and the following linearized output dynamics with linear system coordinates  $\xi = (y_s^T, \dot{y}_s^T)^T$ ,

$$\dot{\xi} = \underbrace{\begin{bmatrix} 0 & I \\ 0 & 0 \end{bmatrix}}_{F} \xi + \underbrace{\begin{bmatrix} 0 \\ I \end{bmatrix}}_{G} \nu.$$

We solve the continuous time algebraic Riccati equation,

$$F^T P + PF - PGG^T P + Q = 0,$$

for this linear system with user-selected weighting matrix  $Q=Q^T>0$ , for  $P=P^T>0$  to construct a RES-CLF per the methods of [10]:

$$\bar{V}_{\varepsilon}^{s}(\xi) = \xi^{T} \begin{bmatrix} \frac{1}{\varepsilon}I & 0 \\ 0 & I \end{bmatrix} P \begin{bmatrix} \frac{1}{\varepsilon}I & 0 \\ 0 & I \end{bmatrix} \xi =: \xi^{T} P^{\varepsilon} \xi.$$

Taking the derivative gives the convergence constraint:

$$\dot{\bar{V}}_{\varepsilon}^{s}(\xi,\nu) = L_{F}\bar{V}_{\varepsilon}^{s}(\xi) + L_{G}\bar{V}_{\varepsilon}^{s}(\xi)\nu \le -\frac{1}{\varepsilon}\frac{\lambda_{min}(Q)}{\lambda_{max}(P)}\bar{V}_{\varepsilon}^{s}(\xi),$$

with Lie derivatives along the linearized output dynamics as,

$$L_F \bar{V}_{\varepsilon}^s(\xi) = \xi^T (F^T P_{\varepsilon} + P_{\varepsilon} F) \xi,$$
  

$$L_G \bar{V}_{\varepsilon}^s(\xi) = 2 \xi^T P_{\varepsilon} G.$$

**ID-CLF-QP+** $F_f$ **.** We can write this RES-CLF and its derivative in terms of x and  $\mathcal X$  to use in the ID-CLF-QP since  $\xi$ 

depends on  $x_s$  through  $y_s(x_s)$  and  $\dot{y}_s(x_s)$  and the relationship in (13) shows  $\nu$  depends on  $\mathcal{X}$ :

$$\nu = L_{\bar{f}^s}^2 y_s(\mathcal{X}) + L_{\bar{g}^s} L_{\bar{f}^s} y_s(\mathcal{X}) u_s(\mathcal{X}). \tag{14}$$

We hence obtain the subsystem RES-CLF (10) with  $\bar{c}_1^s = \lambda_{min}(P)$ ,  $\bar{c}_2^s = \lambda_{max}(P)$ , and  $\bar{c}_3^s = \frac{\lambda_{min}(Q)}{\lambda_{max}(P)}$ . To avoid the matrix inversions required by (14), we use

To avoid the matrix inversions required by (14), we use the facts that  $\nu = \ddot{y}_s$  and the output  $y_s(x_s)$  is a positional constraint, i.e.  $y_s(\bar{q})$ , to write the  $\ddot{y}_s$  in terms of the robotic subsystem's configuration coordinates  $\bar{q}$ :

$$\ddot{y}_{s} = \underbrace{\frac{\partial}{\partial \bar{q}} \left( \frac{\partial \bar{y}_{s}}{\partial \bar{q}} \dot{\bar{q}} \right)}_{\dot{j}_{u}(\bar{q},\dot{\bar{q}})} \dot{\bar{q}} + \underbrace{\frac{\partial y_{s}}{\partial \bar{q}}}_{J_{y}(\bar{q})} \ddot{\bar{q}}. \tag{15}$$

This formulation equates to (14), as shown by [13].

To prescribe a PD controller to  $\ddot{y}$  with a control input  $u_s$  close to (13), we define  $\nu=K_py^s(x_s)+K_d\dot{y}^s(x_s):=\nu_{\rm pd}$  and minimize the difference between  $\nu_{\rm pd}$  and (15) in the QP cost. We also include the holonomic constraints in the cost as soft constraints since these are difficult to satisfy precisely on hardware. With decision variables  $\Upsilon=(\ddot{q}^T,u_s^T,\bar{\lambda}_h^T,\delta)^T\in\mathbb{R}^{\eta_v}$ , with  $\eta_v=\bar{\eta}+m_s+\bar{\eta}_h+1$ , and using the terms,

$$J_c(\bar{q}) = \begin{bmatrix} J_y(\bar{q}) \\ \bar{J}_h(\bar{q}) \end{bmatrix}, \qquad \dot{J}_c(\bar{q}, \dot{\bar{q}}) = \begin{bmatrix} \dot{J}_y(\bar{q}, \dot{\bar{q}}) \\ \dot{J}_h(\bar{q}, \dot{\bar{q}}) \end{bmatrix},$$

we formulate our **ID-CLF-QP+** $F_f$ :

$$\Upsilon^* = \underset{\Upsilon \in \mathbb{R}^{\eta_v}}{\operatorname{argmin}} \left\| \left| \dot{J}_c(\bar{q}, \dot{\bar{q}}) \dot{\bar{q}} + J_c(\bar{q}) \ddot{\bar{q}} - \mu^{\operatorname{pd}} \right| \right|^2 + \sigma W(\Upsilon) + \rho \delta 
\text{s.t. } \bar{D}(\bar{q}) \ddot{\bar{q}} + \bar{H}(\bar{q}, \dot{\bar{q}}) = \bar{B}u_s + \bar{J}_h^T(\bar{q}) \bar{\lambda}_h + \bar{J}_f^T(\bar{q}) F_f 
L_F \bar{V}_\varepsilon^s(\mathcal{X}) + L_G \bar{V}_\varepsilon^s(\mathcal{X}) \left( \dot{J}_y \dot{\bar{q}} + J_y \ddot{\bar{q}} \right) \leq -\frac{\gamma}{\varepsilon} \bar{V}_\varepsilon^s(\mathcal{X}) + \delta 
- u_{\max} \leq u_s \leq u_{\max}.$$
(16)

Here  $\mu^{\mathrm{pd}}=(\nu_{\mathrm{pd}}^{T},0^{T})^{T}$ , the regularization term  $W(\Upsilon)$  makes the system well-posed,  $\sigma$  and  $\rho$  are user-selected weights, and the relaxation term  $\delta$  ensures the torque bounds  $(-u_{\mathrm{max}},u_{\mathrm{max}})$  are always feasible. (We leave out the arguments on  $J_{y},\dot{J}_{y}$  for notational simplicity.)

### B. Controller Realization for Hardware

While [15] realized a variation of the ID-CLF-QP+ $F_f$ , this method was only applied in stance, relied on a force estimation method for  $F_f$ , and used the holonomic constraint wrench  $\bar{\lambda}_h$  for the GRFs. This rigid-contact model used for the GRFs does not hold for a foot contacting a variety of real-world non-rigid terrains. To overcome these limitations, this paper incorporated an IMU, load cell, and insole pressure sensor into the prosthesis platform.

**Sensor Measurements to Complete Dynamics.** While the floating base positions and velocities can still be obtained in stance by inverse kinematics with the prosthesis joint positions and velocities, we use an IMU on the human leg adapter to measure the floating base y-rotation and angular velocity in swing. These measurements with the kinematics give the x and z-Cartesian velocities. The x and z-Cartesian positions do not affect the dynamics and hence are not required. This paper employed a 6-axis load cell to directly

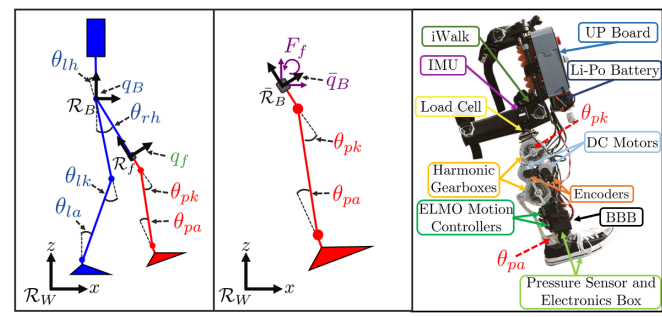


Fig. 2. (Left) The separable human-prosthesis system with full system configuration coordinates. (Middle) The prosthesis equivalent subsystem with subsystem configuration coordinates. (Right) Transfemoral powered prosthesis AMPRO3 with labeled hardware components.

measure the interaction forces  $F_f$  between the human and prosthesis and an insole pressure sensor, detailed in Section V, to determine the vertical GRF  $F_{g,z}$  and pitch ground reaction moment  $M_{g,y}$ . The only remaining unknown force is the horizontal GRF. We solve for the wrench  $\lambda_{h,x} \in \mathbb{R}^1$  through a holonomic constraint, assuming the foot does not slip on the ground.

**ID-CLF-QP+** $F_f$ **+** $\tilde{F}_g$ **.** The final controller formulation is

$$\Upsilon^* = \underset{\Upsilon \in \mathbb{R}^{\eta_v}}{\operatorname{argmin}} \left\| \dot{J}_c(\bar{q}, \dot{q}) \dot{q} + J_c(\bar{q}) \ddot{q} - \mu^{\text{pd}} \right\|^2 + \sigma W(\Upsilon) + \rho \delta 
\text{s.t. } \bar{D}(\bar{q}) \ddot{q} + \bar{H}(\bar{q}, \dot{q}) = \bar{B}u_s + \bar{J}_h^T(\bar{q}) \tilde{F}_g + \bar{J}_f^T(\bar{q}) F_f 
L_F \bar{V}_\varepsilon^s(\mathcal{X}) + L_G \bar{V}_\varepsilon^s(\mathcal{X}) (\dot{J}_y \dot{q} + J_y \ddot{q}) \le -\frac{\gamma}{\varepsilon} \bar{V}_\varepsilon^s(\mathcal{X}) + \delta 
- u_{\text{max}} \le u_s \le u_{\text{max}}.$$
(17)

with modified set of decision variables  $\tilde{\Upsilon} = (\ddot{q}^T, u_s^T, \bar{\lambda}_{h,x}, \delta)^T \in \mathbb{R}^{\tilde{\eta}_v}$  and  $\tilde{\eta}_v = \bar{\eta} + m_s + 2$ . The decision variable  $\bar{\lambda}_{h,x}$  is included with the measured GRFs  $F_{g,z}$  and  $M_{g,y}$  in  $\tilde{F}_g = (\bar{\lambda}_{h,x}, F_{g,z}, M_{g,y})^T$ .

# IV. AMPUTEE-PROSTHESIS MODEL AND GAIT GENERATION

To develop outputs for the human-prosthesis system for the ID-CLF-QP+ $F_f$ + $\tilde{F}_g$ , we construct a model of the system and use hybrid zero dynamics trajectory generation methods.

Amputee-Prosthesis Model. We model an amputee-prosthesis system as a bipedal robot with 8 links and 12 DOFs, i.e.  $\eta=12$  for (1). The prosthesis subsystem has coordinates  $q_s=(\theta_{pk},\,\theta_{pa})^T$  for the knee and ankle pitch respectively, making  $\eta_s=2$ . The remaining amputee system has coordinates  $q_l=(q_B^T,\theta_{lh},\theta_{lk},\theta_{la},\theta_{rh})^T$  defining the floating base at the torso and the left hip, left knee, left ankle, and left hip pitch joints respectively. The fixed joint coordinates  $q_f$  define the interface between the amputee's partial thigh and the top of the prosthesis. See Fig. 2. Every non-fixed joint is actuated, giving  $m_s=2$  and  $m_T=4$ .

The human subject's height and weight along with human inertia, limb mass, and limb length percentage data from [23], [24] provide the human parameters. We base the prosthesis model parameters on the CAD model of AMPRO3 [25], the transfemoral powered prosthesis used in this work. This full system model gives the dynamics of (1) for trajectory generation, for which we omit the ankles since a varying set point PD controller is more comfortable for the user than a prescribed trajectory. The prosthesis equivalent

subsystem is constructed with floating based coordinates  $\bar{q}_B$  at the socket and (3) gives the dynamics used in (17).

Hybrid Systems and Human-Like Gait Generation. Because bipedal walking contains both discrete and continuous dynamics, we model the amputee-prosthesis system as a hybrid system [26]. Since the amputee-prosthesis system is asymmetrical, we consider two domains of continuous dynamics (1)  $\mathcal{D}_v$  with indices  $v \in \{\mathrm{ps,pns}\}$  for prosthesis stance and for prosthesis non-stance, respectively. Each domain has a 3 dimensional holonomic constraint for the respective stance foot ground contact in addition to the fixed joint constraint. Events connect these domains together in a directed cycle, specifically the event of the non-stance foot contacting the ground. The work of [27] explains the impact dynamics occurring at foot-strike.

To design output trajectories for the amputee-prosthesis system that are invariant through impact, we use a hybrid zero dynamics condition [28] in an optimization whose solution must also satisfy the dynamics and feasibility constraints. We design the cost function to minimize the difference between the outputs (the joints) and human walking data obtained through motion capture [29]. The optimization yields parameters for each domain  $\alpha_v$  that define Bézier polynomials for the desired trajectories  $y_{s,v}^d(\tau(x_s),\alpha_v)$  parameterized by the state-based phase variable  $\tau(x_s)$ , forward hip position, which goes from 0 to 1 in each domain  $\mathcal{D}_v$ [28]. Details given [29]. The resulting trajectories match the human data well and are shown in [15]. Since the optimization gives a prosthesis trajectory that matches human walking data and is stable with the human side emulating the human data, we assume in practice the human will still be able to stabilize itself with the prosthesis following this human-like trajectory. This satisfies the required condition about the human for our main theoretical idea in II to ensure full human-prosthesis system stability for a RES-CLF controlling the prosthesis.

# V. PLANTAR PRESSURE SENSOR FOR REAL-TIME FEEDBACK

The prosthesis platform with the new sensors used in this study will be described in VI. First, we will give details here of the pressure sensor selection and use due to the novelty of incorporating plantar pressure data as real-time force input to a model-dependent controller.

**Pressure Sensor Selection.** The pressure sensor used for this study met the restrictive real-time control requirements for our application. Most commercially available insole pressure sensors are designed for recording data for offline gait analysis and are incompatible with our application. First, many insole sensors communicate wirelessly through WiFi or Bluetooth which would introduce a large time-delay, negatively influencing the feedback's effect in real-time control. Second, most companies design pressure sensors with proprietary gait analysis software and the raw data is inaccessible in real-time for custom use. Finally, most wired pressure sensor systems are very expensive, \$10-35k. The sensor for this study is

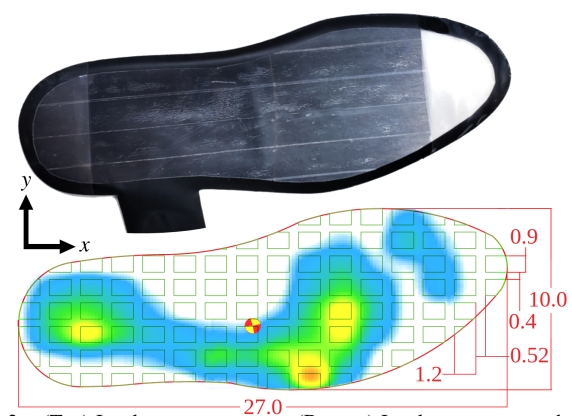


Fig. 3. (Top) Insole pressure sensor. (Bottom) Insole sensor array drawing with dimensions in cm and overlay of colored pressure map from the Tactilus software. The circular marker indicates the CoP estimate.

\$2.5-3k and a company-provided API accesses the raw data in real-time over a USB connection.

**Pressure Sensor Hardware.** The pressure sensor used is a SensorProd Inc. Tactilus Foot Insole Sensor System, High-Performance V Series (SP049), shown in Fig. 3. The sensor is reversible and can be placed in the shoe of either foot. A small electronics box attached to the sensor extends a few inches off of the sensor and can be strapped to the user's or prosthesis's calf. Made of a piezoresistive sensor array, the insole pressure sensor can sense up to 206.8 kPa at 101 separate points per foot. Each sensor element is 0.9 cm ×  $1.2~\mathrm{cm}~\times~0.127~\mathrm{cm}$  in size and has a column pitch of 1.3cm and a row pitch of 1.72 cm over a total insole size of  $10.0 \text{ cm} \times 27.0 \text{ cm}$ , as shown in Fig. 3. The sensor elements are arranged as a 16×8 matrix, although some elements are not present on the insole and give vacuous readings. The sensor provides a resolution of  $\pm 1~\mu$ Pa with 12 significant digits at most, along with an accuracy of  $\pm 10\%$ , repeatability of  $\pm 2\%$ , hysteresis of  $\pm 5\%$ , and a non-linearity of  $\pm 1.5\%$ . To interface with the pressure sensor, we use an UP Board (02/32), which is a small x86 single-board computer with 40-pins for general-purpose input and output and 4 USB ports. We selected the UP board for its small form factor and capability to run a Windows OS to use the sensor's API.

**Pressure Sensor Software.** We incorporated the Tactilus API, a precompiled C++ Windows Library from SensorProd Inc., into a Windows C++ program which scanned the pressure readings in real time at about 200 Hz with the UP Board through a USB connection. We applied a Gaussian smoothing filter to reduce high differences in pressure readings between adjacent sensor elements potentially due to falsely concentrated readings. This common non-uniform low-pass filter convolves each pressure reading  $\mathcal{P}_{i,j}$  of sensor element in row i and column j with the matrix

$$\mathcal{G} = \begin{bmatrix} \frac{1}{16} & \frac{1}{8} & \frac{1}{16} \\ \frac{1}{8} & \frac{1}{4} & \frac{1}{8} \\ \frac{1}{16} & \frac{1}{8} & \frac{1}{16} \end{bmatrix}.$$

Every pressure reading  $\mathcal{P}_{i,j}$  is replaced by the filtered reading

 $\tilde{\mathcal{P}}_{i,j}$ , a weighted sum of itself and its surrounding readings:

$$[\tilde{\mathcal{P}}]_{ij} = \sum_{a=i-1}^{i+1} \sum_{b=j-1}^{j+1} \mathcal{G}_{(a-i+2)(b-j+2)} \mathcal{P}_{ab}.$$

At the edges a partial G matrix is used with scaled up weights that sum to 1. To reduce the effect of environmental and systematic high-frequency noise in time, we apply a simple moving average to each  $\tilde{\mathcal{P}}_{i,j}$  giving us  $\tilde{\mathcal{P}}_{i,j}^{\mathrm{avg}}$ .

With  $\tilde{\mathcal{P}}_{i,j}^{\mathrm{avg}}$ , we calculate total vertical GRF  $F_{g,z}$ :

$$F_{g,z} = \sum_{i=1}^{16} \sum_{j=1}^{8} w_{ij} \tilde{\mathcal{P}}_{i,j}^{\text{avg}} \Delta \mathbf{x} \Delta \mathbf{y}, \tag{18}$$

where  $\Delta x$  is the sensor element row pitch,  $\Delta y$  the column pitch, and  $w_{i,j}$  a weighting factor based on the approximate percentage of remaining rectangular sensor element. Fig. 3 shows the edge elements are partial rectangles. The numbers 16 and 8 are the total number of rows and columns, respectively. The sensor elements not present on the insole return 0 readings. We obtain the moment by,

$$M_{g,y} = \sum_{i=1}^{16} (\mathbf{x}_0 - \mathbf{x}_i) \sum_{j=1}^{8} w_{ij} \tilde{\mathcal{P}}_{i,j}^{\text{avg}} \Delta \mathbf{x} \Delta \mathbf{y},$$
 (19)

where  $x_i$  is the x-position of the sensor and  $x_0$  is the x-position of the selected point of rotation, in this case directly below the center of rotation of the ankle.

### VI. HUMAN-PROSTHESIS EXPERIMENTATION

We integrated the pressure sensor along with a load cell and IMU into a current powered prosthesis platform to achieve model-based prosthesis control with real-time in-theloop forcing sensing. The stable human-prosthesis walking results are presented here.

**Prosthesis Platform AMPRO3.** This study uses the transfemoral powered prosthesis platform AMPRO3 custom-built and introduced in [25]. Two brushless DC motors (MOOG BN23) with 1 Nm peak torque actuate the knee and ankle pitch joints through their interactions with their respective timing belt connected to each joint's harmonic gear box. This gear reduction system gives a 120:1 mechanical reduction for the knee and 175:1 for the ankle.

The motors are controlled by 2 ELMO motion controllers (Gold Solo Whistle) which receive position and velocity feedback from the 2 incremental encoders, which the motion controllers send to the microprocessor. The microprocessor returns a commanded torque to the motion controllers. The controller algorithms run on the Beaglebone Black Rev C (BBB) microprocessor at 166Hz and are coded in C++ packages with ROS. The coded ID-CLF-QP+ $F_f$ + $\tilde{F}_g$  is based on code from [13].

The insole sensor is physically integrated into the prosthetic system through placement over the insole of a Converse All-Star Men's Size 9 Wide shoe which is worn by the foot of AMPRO3. This shoe has a flat, stiff sole, allowing the sensor to lie flat and be more sensitive to pressure changes during a step. The sensor connects to the UP Board through

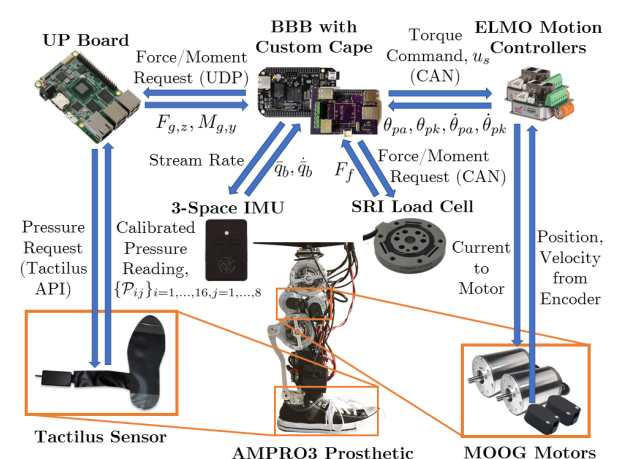


Fig. 4. Hardware and software flow diagram depicting how the pressure sensor, load cell, and IMU communicate and interact with the prosthesis control scheme.

USB, and sends force and moment measurements to the BBB through UDP over Ethernet. There is a 5 ms time delay between when the sensor pressure is read and the BBB receives the data caused largely by the time it takes the Windows program to receive all the data from the sensor.

A Yost Labs 3-Space<sup>TM</sup> Sensor USB/RS232 IMU is mounted to the side of the human leg adapter on the prosthesis platform. This connects to the BBB via USB and streams data at 750 Hz. A 6-axis load cell (M3564F, Sunrise Instruments) is mounted at the interface between the proximal end of the prosthesis knee joint and distal end of the human leg adapter with custom designed aluminum parts. The load cell can measure forces/moments along the x and y-axes up to 2500 N/200 Nm and z-axis up to 5000 N/100 Nm. A signal conditioning box (M8131 Sunrise Instruments) connects to the BBB with a custom-designed cape and sends data and sends new data via CAN communication once every control loop. A newly designed electronics box mounted on the iWalk houses the load cell box, UP Board, and a 9cell 4400 mAh Li-Po battery (Thunder Power RC) which powers the whole system. Fig. 2 shows AMPRO3 with the aforementioned components labeled and Fig. 4 shows a software flow diagram.

Hardware Results. A 1.7 m, 62 kg non-amputee human subject tested the prosthesis device with an iWalk adapter. The iWalk allows her bent right leg to be strapped to the device for walking as shown in Fig. 1. A foam shoe lift strapped to the bottom of her left leg's shoe evens the length difference between her own left leg and her right leg with the prosthesis. A moving average time window of 2 for the pressure sensor filter sufficed to provide smooth signals to the controller. No filter was used for the load cell. We applied the proposed controller to the knee in both stance and non-stance phase. A PD controller with varying set-point was applied to the prosthesis ankle.

The subject walked with the prosthesis for at least 30 steps with 2 different controllers on four types of terrain: a rubber floor, an outdoor track, grass, and a sidewalk, Fig. 5. The first controller is the ID-CLF-QP+ $F_f$ + $\tilde{F}_g$  (17), the controller of focus in this paper, using the pressure sensor to obtain  $F_{g,z}$ 



Fig. 5. Gait tiles of experiments on 4 terrains. From top to bottom: rubber floor, outdoor track, grass, sidewalk.

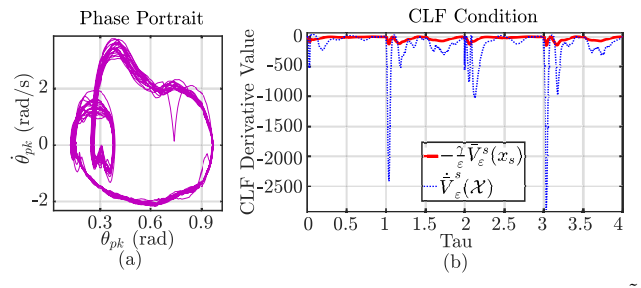


Fig. 6. (a) Phase portrait of first 18 steps using the ID-CLF-QP+ $F_f$ + $F_g$  controller (17) on a sidewalk, showing the system yields a stable periodic orbit. (b) CLF bound and derivative for first 4 steps of the same experiment, showing the prosthesis usually satisfies the stability condition.

(18),  $M_{g,y}$  (19), the load cell to obtain  $F_f$ , and the IMU in swing for  $\bar{q}_B$  and  $\dot{\bar{q}}_B$ . For comparison, we tested an ID-CLF-QP without including the measurements from the pressure sensor, load cell, and IMU to see the effect the sensor measurements have on the controller performance. Here the GRFs were determined with the holonomic constraints (4) but the fixed joint forces were considered 0. The gains  $\nu_{\rm pd}$  and all other user-selected terms in the QP were kept consistent between controllers.

The knee phase portrait of Fig. 6 a. shows the stability of this main controller for 18 steps on a sidewalk. Fig. 6 b. depicts the CLF derivative with its upper CLF stability bound for the first 4 steps. While the derivative occasionally exceeds the bound because of the relaxation term in the QP (17), the overall human-prosthesis system can still be input-to-state stable as proved in [30]. Additionally, although the force measurements may have error from sensor noise and time delay, the work of [30] showed for a bounded error in the force measurement the prosthesis will still be stable to a set and conditions exist such that the human will remain exponential input-to-state stable [31] when the prosthesis deviates from its nominal control law.

Fig. 7 a. shows the mean torque inputs with 3 standard deviations of these two controllers for 14 steps on 4 different terrains. Both controllers exhibit variation between steps on a given terrain and variation between terrains. However the

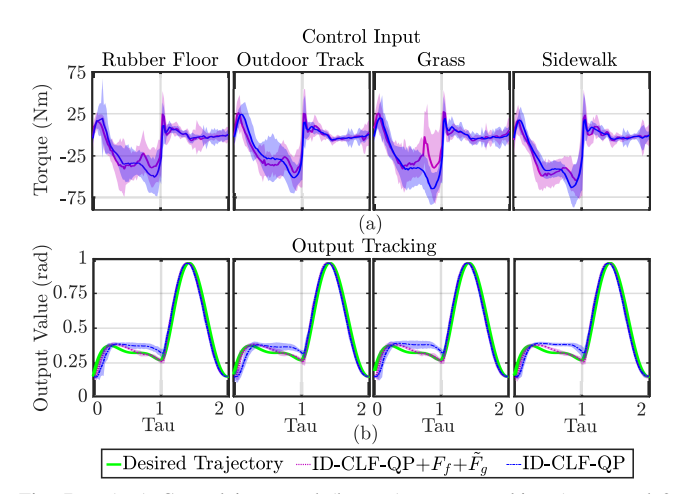


Fig. 7. (top) Control input and (bottom) output tracking (mean and 3 standard deviations) with ID-CLF-QP+ $F_f+\tilde{F}_g$  and the ID-CLF-QP without force sensors for four different terrains for 14 steps.

variation in the ID-CLF-QP+ $F_f+\tilde{F}_g$  leads to better tracking performance than the ID-CLF-QP with no force sensors. Fig. 7 b. depicts the tracking performance with the mean and 3 standard deviations. Both controllers track well in swing phase, but the ID-CLF-QP+ $F_f+\tilde{F}_g$  achieves better tracking in stance than the ID-CLF-QP on all terrains and has a smaller standard deviation along the trajectories. In terms of tracking, the ID-CLF-QP+ $F_f+\tilde{F}_g$  also outperforms the PD controller used in [15].

These results show the ID-CLF-QP+ $F_f$ + $F_g$  can achieve better and more consistent tracking with use of these force sensors than without, suggesting that accounting for the forces in the dynamics allows this model-dependent controller to respond to its real-time loading conditions to achieve good tracking. This also suggests the improvement in model accuracy allows this model-dependent controller to better capture the nonlinearities of a trajectory, motivating using model-dependent prosthesis controllers to achieve more dynamic behaviors. This motivates further study of model-dependent prosthesis control methods to assess if the model-dependence can yield a more transferable method between prosthetic devices and users, requiring less tuning and yielding formal guarantees of stability.

### VII. CONCLUSION AND FUTURE WORK

This work achieved the first experimental realization of a model-dependent prosthesis controller in both stance and swing using real-time in-the-loop force measurements to complete the dynamics using an insole pressure sensor, load cell, and IMU resulting in stable human-prosthesis walking. This controller achieved better and more consistent tracking on 4 types of terrain compared to its counterpart without force sensors and the PD controller in [15]. This demonstrates this controller's robustness and ability to adapt to varying loading conditions. This suggests model-dependence can be used to overcome the need to tune many parameters for every user and behavior as is required in typical impedance prosthesis control methods, providing a more transferable method between users and behaviors and reducing the time amputees spend in a tuning session.

Integration of the insole pressure sensor into the prosthesis platform opens the door to future work accounting for gait stability measures such as CoP in model-dependent prosthesis control methods and gait analysis [32], [33]. Additionally, by removing most of the rigid contact assumption and directly measuring the forces from the human and ground with the load cell and pressure sensor, we enable the prosthesis to account for its real-world conditions. These sensing methods increase the validity of our human-prosthesis stability guarantees and could empower a variety of amputees to walk in varying ways across changing terrain.

Future work will test more subjects to further assess this controller's ability to consistently achieve good tracking performance while undergoing different loading conditions. To improve the controller's ability to consistently meet the Lyapunov stability condition shown in 6, we could increase the weight of the relaxation term in (17) and decrease  $\varepsilon$  to increase the convergence rate. Additionally implementing the ESS-ID-CLF-QP of [30] could reduce the effects of force measurement error and reduce the set size the prosthesis converges to. This controller will also be used to achieve multi-contact prosthesis to yield a more natural and dynamic gait. Having access to a CoP measurement enables use of CoP as phase variable [5] and could be used as a guard to determine transitions in multi-domain multi-contact walking [34] for more efficient and human-like walking. Having this insole pressure sensor also allows incorporation of other plantar pressure data into our control methods and gait analysis to increase stability and prosthesis reactivity.

#### REFERENCES

- [1] E. L. Bukowski, "Atlas of Amputations and Limb Deficiencies: Surgical, Prosthetic, and Rehabilitation Principles, ed 3," *Physical Therapy*, vol. 86, no. 4, pp. 595–596, 04 2006.
- [2] J. Kulkarni, S. Wright, C. Toole, J. Morris, and R. Hirons, "Falls in patients with lower limb amputations: Prevalence and contributing factors," *Physiotherapy*, vol. 82, no. 2, pp. 130–136, 1996.
- [3] J. Johansson, D. Sherrill, P. Riley, P. Bonato, and H. Herr, "A clinical comparison of variable-damping and mechanically passive prosthetic knee devices," *American journal of physical medicine & rehabilitation* / *Association of Academic Physiatrists*, vol. 84, pp. 563–75, 09 2005.
- [4] F. Sup, A. Bohara, and M. Goldfarb, "Design and control of a powered transfemoral prosthesis," *The International Journal of Robotics Research*, vol. 27, no. 2, pp. 263–273, 2008, pMID: 19898683.
- [5] R. D. Gregg, T. Lenzi, L. J. Hargrove, and J. W. Sensinger, "Virtual constraint control of a powered prosthetic leg: From simulation to experiments with transfemoral amputees," *IEEE Transactions on Robotics*, vol. 30, no. 6, pp. 1455–1471, Dec 2014.
- [6] B. E. Lawson, H. A. Varol, A. Huff, E. Erdemir, and M. Goldfarb, "Control of stair ascent and descent with a powered transfermoral prosthesis," *IEEE Transactions on Neural Systems and Rehabilitation Engineering*, vol. 21, no. 3, pp. 466–473, 2013.
- [7] A. Simon, K. Ingraham, N. Fey, S. Finucane, R. Lipschutz, A. Young, and L. Hargrove, "Configuring a powered knee and ankle prosthesis for transfemoral amputees within five specific ambulation modes," *PloS one*, vol. 9, p. e99387, 06 2014.
- [8] S. K. Au, J. Weber, and H. Herr, "Powered ankle-foot prosthesis improves walking metabolic economy," *IEEE Transactions on Robotics*, vol. 25, no. 1, pp. 51–66, 2009.
- [9] R. Gehlhar and A. D. Ames, "Separable control lyapunov functions with application to prostheses," *IEEE Control Systems Letters*, vol. 5, no. 2, pp. 559–564, 2021.
- [10] A. D. Ames, K. Galloway, K. Sreenath, and J. W. Grizzle, "Rapidly exponentially stabilizing control Lyapunov functions and hybrid zero dynamics," *IEEE Transactions on Automatic Control*, vol. 59, no. 4, pp. 876–891, 2014.

- [11] A. E. Martin and R. D. Gregg, "Stable, robust hybrid zero dynamics control of powered lower-limb prostheses," *IEEE Transactions on Automatic Control*, vol. 62, no. 8, pp. 3930–3942, 2017.
- [12] R. Gehlhar, J. Reher, and A. D. Ames, "Control of separable subsystems with application to prostheses," arXiv preprint arXiv:1909.03102, 2019.
- [13] J. Reher, C. Kann, and A. D. Ames, "An inverse dynamics approach to control lyapunov functions," in 2020 American Control Conference (ACC), 2020, pp. 2444–2451.
- [14] Å. Björck, "Numerical methods for least square problems," 1996.
- [15] R. Gehlhar and A. D. Ames, "Model-dependent prosthesis control with interaction force estimation," in 2021 IEEE International Conference on Robotics and Automation, 2021.
- [16] X. Xiong, A. D. Ames, and D. I. Goldman, "A stability region criterion for flat-footed bipedal walking on deformable granular terrain," in 2017 IEEE/RSJ International Conference on Intelligent Robots and Systems (IROS). IEEE, 2017, pp. 4552–4559.
- [17] F. Sup, H. A. Varol, J. Mitchell, T. Withrow, and M. Goldfarb, "Design and control of an active electrical knee and ankle prosthesis," in 2008 2nd IEEE RAS EMBS International Conference on Biomedical Robotics and Biomechatronics, 2008, pp. 523–528.
- [18] T. Elery, S. Rezazadeh, C. Nesler, and R. D. Gregg, "Design and validation of a powered knee–ankle prosthesis with high-torque, lowimpedance actuators," *IEEE Transactions on Robotics*, vol. 36, no. 6, pp. 1649–1668, 2020.
- [19] A. Razak, A. Zayegh, R. Begg, and Y. Wahab, "Foot plantar pressure measurement system: A review," *Sensors (Basel, Switzerland)*, vol. 12, pp. 9884–912, 12 2012.
- [20] R. M. Murray, S. S. Sastry, and L. Zexiang, A Mathematical Introduction to Robotic Manipulation, 1st ed. Boca Raton, FL, USA: CRC Press. Inc., 1994.
- [21] G. Taga, "A model of the neuro-musculo-skeletal system for human locomotion," *Biol. Cybern.*, vol. 73, no. 2, p. 113–121, Jul. 1995.
- [22] A. Isidori, Nonlinear Control Systems. Springer London, 1995.
- [23] S. Plagenhoef, F. G. Evans, and T. Abdelnour, "Anatomical data for analyzing human motion," *Research Quarterly for Exercise and Sport*, vol. 54, no. 2, pp. 169–178, 1983.
- [24] W. Erdmann, "Geometry and inertia of the human body review of research," Acta of Bioengineering and Biomechanics, vol. 1, pp. 23– 35, 1999.
- [25] H. Zhao, E. Ambrose, and A. D. Ames, "Preliminary results on energy efficient 3D prosthetic walking with a powered compliant transfemoral prosthesis," in *Robotics and Automation (ICRA)*, 2017 IEEE International Conference on. IEEE, 2017, pp. 1140–1147.
- [26] A. D. Ames, "Human-inspired control of bipedal walking robots," IEEE Transactions on Automatic Control, vol. 59, no. 5, pp. 1115– 1130, 2014.
- [27] J. W. Grizzle, C. Chevallereau, R. W. Sinnet, and A. D. Ames, "Models, feedback control, and open problems of 3d bipedal robotic walking," *Automatica*, vol. 50, no. 8, pp. 1955 – 1988, 2014.
- [28] E. R. Westervelt, J. W. Grizzle, C. Chevallereau, J. H. Choi, and B. Morris, Feedback control of dynamic bipedal robot locomotion. CRC press, 2018.
- [29] R. Gehlhar, Y. Chen, and A. D. Ames, "Data-driven characterization of human interaction for model-based control of powered prostheses," in 2020 IEEE/RSJ International Conference on Intelligent Robots and Systems (IROS), 2020, pp. 4126–4133.
- [30] R. Gehlhar and A. D. Ames, "Estimate-to-state stability for hybrid human-prosthesis systems," in (To appear in) 2021 IEEE International Conference on Decision and Control, 2021.
- [31] E. D. Sontag and Y. Wang, "On characterizations of the input-to-state stability property," *Systems & Control Letters*, vol. 24, no. 5, pp. 351– 359, 1995.
- [32] C. Kendell, E. Lemaire, N. Dudek, and J. Kofman, "Indicators of dynamic stability in transtibial prosthesis users," *Gait & Posture*, vol. 31, no. 3, pp. 375–379, 2010.
- [33] M. Schmid, G. Beltrami, D. Zambarbieri, and G. Verni, "Centre of pressure displacements in trans-femoral amputees during gait," *Gait & Posture*, vol. 21, no. 3, pp. 255–262, 2005.
- [34] H. Zhao, J. Horn, J. Reher, V. Paredes, and A. D. Ames, "Multicontact locomotion on transfemoral prostheses via hybrid system models and optimization-based control," *IEEE Transactions on Automation Science and Engineering*, vol. 13, no. 2, pp. 502–513, April 2016.